13th International Symposium on Particle Image Velocimetry – ISPIV 2019
Munich, Germany, July 22-24, 2019

PIV-based pressure and stress field measurement for non-Newtonian flow fields

Yuichi Murai[1]*, Neetu Tiwari[1], Hyun Jin Park[1], Yuji Tasaka[1]

[1]Hokkaido University, Faculty of Engineering, Sapporo, Hokkaido, Japan

*murai@eng.hokudai.ac.jp

Abstract

Simultaneous estimation of pressure and stress field of a shear-thinning fluid is conducted by means of particle image velocimetry, applied for vortex shedding flow behind a circular cylinder. Governing equation generalized for non-Newtonian fluid is coupled with PIV data. The result shows feasibility of the method and also a specific feature of the flow such as vortex-dependent viscosity that takes place in the acceleration process of the wake.

1 Introduction

Non-Newtonian fluids are ubiquitous in industrial and biological processes. The rheological properties of these fluids are generally evaluated by 'flow curve' produced by rheometers (Cross, 1968). Based on these measurements, rheological models such as power law, Carreau model (Carreau, 1972), Herschel-Berkley, etc. are introduced to the analysis of flow. With numerical simulations, these models improved our understanding of complex fluid behavior in many practical flows (Clermont and Normandin, 1993). However, it is still a challenge for computational rheologists to predict the material behavior during fluid-structure interaction in complex flow geometries (Walters and Webster, 2003). In particular, non-Newtonian flow behaviors coupled with vortex dynamics cannot be predicted by simple rheological models. The difficulty originates from potential interaction between pressure and viscosity fields.

Flow of non-Newtonian fluids are also studied by velocity measurement devices, like Laser Doppler Velocimeter (LDV)(Tamano et al., 2010), Ultrasonic Velocity Profiler (UVP) (Shiratori et al., 2015)(Yoshida et al., 2017)(Tasaka et al., 2018), and Particle Image Velocimetry (PIV)(Yip et al. 2011)(Dey et al., 2018). These techniques are helpful to visualize non-Newtonian fluid flow structures quantitatively to assess the influence of fluid rheology. For pressure driven flows, UVP-PD (Ultrasonic Velocity Profiler combined with pressure drop measurement) (Wiklund et al. 2008) is an effective tool for in-line rheometry suitable for pipe flows. The pressure measurement at two points and velocity measurement are enough for viscosity calculation. For external flow problems, in contrast, two-dimensional (2D) pressure distribution needs to be introduced along with velocity measurements for coupling with rheological study. However, measurement of pressure distribution in arbitrary fluid space is still an unsolved challenge, especially for non-Newtonian fluid flows.

For Newtonian fluid flows, various approaches for pressure estimation based on PIV have been developed in the last decade (van Oudheusden, 2013)(van der Kinere et al., 2019). One of the

present authors have used this technique on flow around rotating turbines (Murai et al., 2007). In this technique the PIV measured velocity data are substituted in one of pressure governing equations: Bernoulli's equation, Navier-Stokes and pressure Poisson equations as written bellow:

$$\frac{1}{2}\rho u_1^{\,2} + p_1 + \rho g z_1 = \frac{1}{2}\rho u_2^{\,2} + p_2 + \rho g z_2 \tag{1}$$

$$\nabla p = -\rho\left\{\frac{\partial \mathbf{u}}{\partial t} + (\mathbf{u}\cdot\nabla)\mathbf{u}\right\} + \mu\nabla^2\mathbf{u} \tag{2}$$

$$\nabla^2 p = -\rho\nabla\cdot(\mathbf{u}\cdot\nabla)\mathbf{u} \quad \rightarrow -2\rho\left(\frac{\partial u}{\partial x}\frac{\partial v}{\partial y} - \frac{\partial u}{\partial y}\frac{\partial v}{\partial x}\right)_{if\,2D} \tag{3}$$

Here, u1 and u2 in Eq. (1) are absolute velocity along a single streamline. ρ, g and z are density, gravitational acceleration and height. In Eqs. (2) and (3), u and μ represent fluid flow velocity vector and viscosity of fluid. Bernoulli's equation, Eq. (1), can be used when flow can be approximated to irrotational flow. Navier-Stokes equation, Eq. (2), gives pressure gradient vector distribution as velocity distribution is measured. By applying divergence in Eq. (2), pressure Poisson equation, Eq. (3), is derived. Since this does not include time derivative term and viscosity term, it can be even applied for unsteady viscous flows. Hence, Poisson equation is widely used for pressure field estimation from PIV data. For non-Newtonian fluids, Eq. (2) must be replaced with a generalized form of momentum conservation equation to which specific rheological model needs to be introduced. Consequently, Eq. (3) becomes invalid for non-Newtonian fluids and additional terms are introduced.

2 Experimental Set-up

A towing tank system was used to study the vortex flow behind a circular cylinder. The experimental arrangements are shown in Fig.1. The dimensions of liquid tank are 5 m in length (l), 0.54 in width (w) and 0.45 m in depth (h). The circular cylinder is made of acrylic glass, of diameter of D = 0.04 m and length of 0.10 m. The circular cylinder is fixed on carriage with vertical shafts. The cylinder is attached horizontally so that Z axis coincides with cylinder axis. The cylinder is positioned at h/2 distance from the upper liquid free surface to ensure no additional effect of the free surface or bottom boundary on the wake of cylinder. The aqueous solution of CMC of 0.1wt % is used as a test fluid which is a shear thinning fluid. The rheological property of the fluid is explained later. Spherical tracer particles are mixed in the liquid for PIV measurement, which are made of high-porous polymer with hydrophilic surface property to aqueous solution (HPSS20, Mitsubishi Chemical). Density and diameter of the particles are 990 kg/m3 and 50-120 μm.

The PIV system consists of one high speed camera with 300 mm Nikkor lens and green laser. The laser beam is expanded to a light sheet illuminating the flow around 3D (three-diameter) downstream of the cylinder. The camera is focused at the wake behind the cylinder in x-y plane. The stands are used to carry the camera and the laser setup. They are towed with the cylinder by the towing carriage system. Towing speed and acceleration are controlled by PC attached to the camera. This enables Lagrangian PIV measurement within the carriage distance of which maximum is 60D. The measurements were performed at carriage speed, U = 0.03 m/s. The images were obtained at

50 fps frame rate. Image processing and PIV were performed using PIVLAB software (Srinivasan and Rajagopal, 2010)(Thielicke and Stamhuis, 2014). The instantaneous velocity data were obtained from two consecutive images by applying FFT based cross-correlation algorithm using recursive approach (Scarano and Riethmuller, 1999) with step-wise interrogation window areas from 128x64, 64x32, and 32x16.

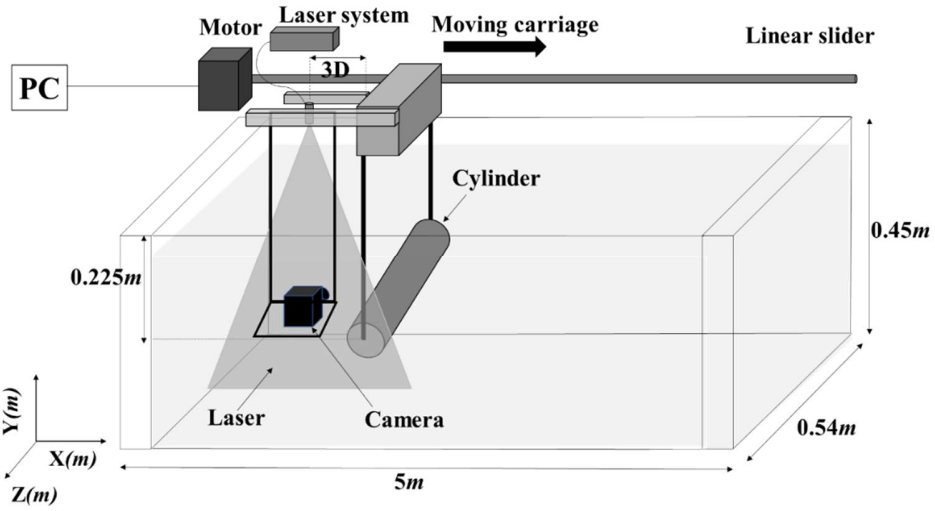

Fig. 1 Experimental arrangement for velocity measurement in wake of fixed cylinder by PIV system

3 Numerical Method

3.1. Governing equations

PIV data are utilized in governing equations of non-Newtonian flow. In description of governing equations, the following scaling variable are used for providing dimensionless terms: D, diameter of cylinder, for length variables, U for velocity terms, and ρU^2 for pressure. Here is density. The dimensionless governing equations in the cartesian coordinates can be written as below:

1) Momentum conservation equation in x and y directions

$$\frac{\partial p}{\partial x} = -\left(u\frac{\partial u}{\partial x} + v\frac{\partial u}{\partial y} \right) + \frac{1}{\mathrm{Re}}\left(\frac{\partial \tau_{xx}}{\partial x} + \frac{\partial \tau_{yx}}{\partial y} \right), \tag{4}$$

$$\frac{\partial p}{\partial y} = -\left(u\frac{\partial v}{\partial x} + v\frac{\partial v}{\partial y} \right) + \frac{1}{\mathrm{Re}}\left(\frac{\partial \tau_{yx}}{\partial x} + \frac{\partial \tau_{yy}}{\partial y} \right). \tag{5}$$

Here Re stands for Reynolds number for non-Newtonian flow, which depends on rheological type of fluids.

2) Relation between shear stress and strain rate

$$\tau_{i,j} = \eta \varepsilon_{i,j}, \tag{6}$$

where, i, j indicates x, y respectively. is non-dimensional viscosity and is non-dimensional strain rate tensor, which is computed by measured velocity field as:

$$\varepsilon_{ij} = \frac{1}{2}\left(\frac{\partial \mathbf{u}_i}{\partial j} + \frac{\partial \mathbf{u}_j}{\partial i} \right) . \tag{7}$$

Substitution of Eqs. (6) and (7) into Eqs. (4) and (5), we can get

$$\frac{\partial p}{\partial x} = -\left(u\frac{\partial u}{\partial x} + v\frac{\partial u}{\partial y} \right) + \frac{\eta}{\mathrm{Re}}\left(\frac{\partial^2 u}{\partial x^2} + \frac{\partial^2 u}{\partial y^2} \right) + \frac{2}{\mathrm{Re}}\left(\varepsilon_{xx}\frac{\partial \eta}{\partial x} + \varepsilon_{yx}\frac{\partial \eta}{\partial y} \right), \tag{8}$$

$$\frac{\partial p}{\partial y} = -\left(u\frac{\partial v}{\partial x} + v\frac{\partial v}{\partial y} \right) + \frac{\eta}{\mathrm{Re}}\left(\frac{\partial^2 v}{\partial x^2} + \frac{\partial^2 v}{\partial y^2} \right) + \frac{2}{\mathrm{Re}}\left(\varepsilon_{xy}\frac{\partial \eta}{\partial x} + \varepsilon_{yy}\frac{\partial \eta}{\partial y} \right). \tag{9}$$

Velocity and strain rate in the r.h.s. of Eqs. (8) and (9) are given by PIV measurement. Hence, pressure gradients and viscosity are obtained by solving these two equations using finite difference method. We adopted central difference scheme to discretize all the terms. Note that no upstream differencing scheme needs to be introduced since velocity is already given experimentally. Thus, Eqs. (8) and (9) belong to ellipsoidal differential equations for pressure and therefore numerical solver for boundary value problem can be applied.

If we derive pressure Poisson equation from Eqs. (8) and (9), it expands like

$$\begin{aligned} \nabla^2 p &= \frac{\partial^2 p}{\partial x^2} + \frac{\partial^2 p}{\partial y^2} \\ &= \frac{\partial}{\partial x}\left\{ -\left(u\frac{\partial u}{\partial x} + v\frac{\partial u}{\partial y} \right) + \frac{\eta}{\mathrm{Re}}\left(\frac{\partial^2 u}{\partial x^2} + \frac{\partial^2 u}{\partial y^2} \right) + \frac{2}{\mathrm{Re}}\left(\varepsilon_{xx}\frac{\partial \eta}{\partial x} + \varepsilon_{yx}\frac{\partial \eta}{\partial y} \right) \right\} \\ &+ \frac{\partial}{\partial y}\left\{ -\left(u\frac{\partial v}{\partial x} + v\frac{\partial v}{\partial y} \right) + \frac{\eta}{\mathrm{Re}}\left(\frac{\partial^2 v}{\partial x^2} + \frac{\partial^2 v}{\partial y^2} \right) + \frac{2}{\mathrm{Re}}\left(\varepsilon_{xy}\frac{\partial \eta}{\partial x} + \varepsilon_{yy}\frac{\partial \eta}{\partial y} \right) \right\}. \end{aligned} \tag{10}$$

Because of complicated source terms composed of higher-order spatial derivatives of velocity, it is hardly computable from PIV data under a limited velocity resolution. Viscosity terms do not disappear as in Newtonian case (Eq. (3)). This means that the advantage of Poisson equation is lost in non-Newtonian flows. We therefore employ Eqs. (8) and (9) for pressure field computations.

4 Results and Discussion

4.1 Viscosity and pressure distributions

The velocity data are reconstructed by considering POD mode 1 to 3 and used in the calculation of II2D (Eq. (14)). This procedure is step ii) described in Section 5. The viscosity distribution at t=12 is calculated using (a) Carreau-Yasuda and (b) power law model and shown in Fig. 2. The viscosity distribution by power law model is qualitatively similar to that by Carreau-Yasuda model. The viscosity is lower in wake region due to higher strain in that region. This result demonstrates shear thinning property of the CMC aqueous solution. However, for free stream region where strain rates are comparatively smaller, the power law model predicted higher viscosity which is quite expected.

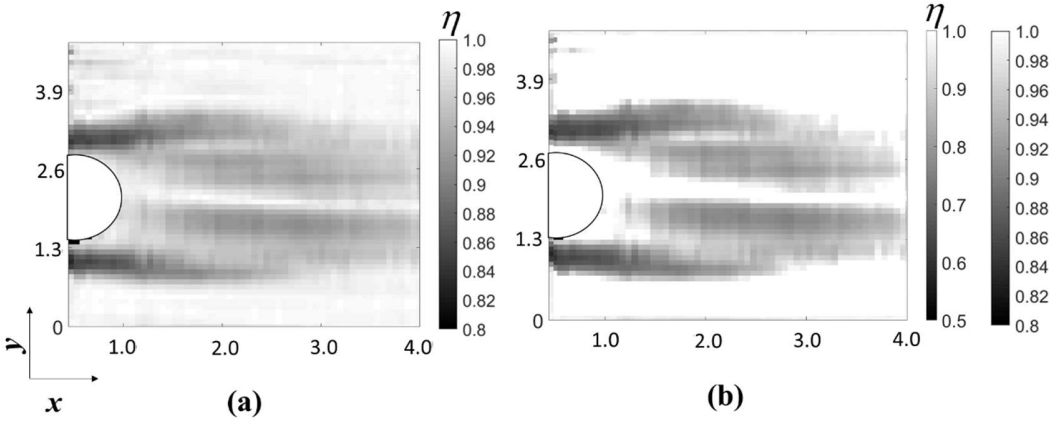

Fig.2 Viscosity distribution in entire computational domain at U = 0.03m/s, t = 12 s, estimated by (a) Carreau-Yasuda model and (b) power law model. (c) Quantitative viscosity distribution calculated by power law model and Carreau -Yasuda for entire computational domain

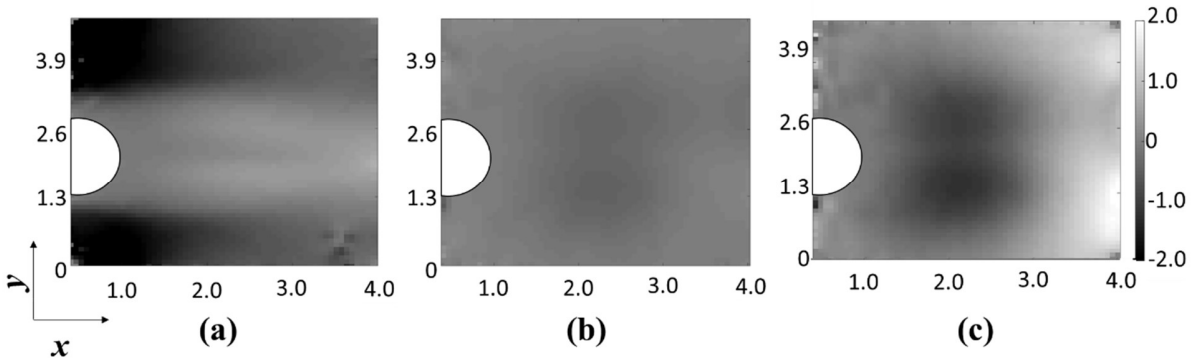

Fig.3 Pressure distribution plots using (a) unfiltered (b) Median filtered (c) POD filtered velocity data at U = 0.03 m/s, t = 12 s

The pressure distributions are obtained by utilizing velocity and viscosity (using Carreau-Yasuda model) in momentum equations are shown in Fig.8. Here Fig. 3(a) represents the pressure distribution obtained by using unfiltered velocity data. The pressure in wake region is higher than other regions which is unrealistic. Using median filtered velocity data on momentum equation, the pressure distribution is shown in Fig. 3(b). With this approach we successfully obtained the low-pressure region in wake although the presence of vortices is still not clear. On the other hand, in Fig. 3(c) pressure distribution by POD filtered data is more realistic. The low-pressure region is formed in the wake, clearly indicating the presence of a pair of vortices behind the cylinder. This procedure is described as step iii) and iv). The momentum equation consists of nonlinear terms and higher order derivatives. The inclusion of rheological data made the equation more susceptible to error amplification. In Fig 3(c) the noise can be seen near the boundaries, but it did not propagate in entire domain while integration of pressure gradients (step iv). This proves that, with suitable POD filtering, adopted numerical scheme is stable and pressure estimation algorithm is robust. Moreover, the three-dimensionality close to cylinder in present experimental condition could be considerable.

Although, error due to 2D assumption of 3D flow is limited to 5% for pressure in wake of a cylinder upto Re=1600 (McLcure and Yarusevych, 2017). This is attributed to the understanding that the energy containing dynamic part of vortex shedding flow is mostly 2D while vortex filaments are distributed in 3D. In addition, POD analysis included the lower modes containing high energy content of flow.

4.2 Performance of Algorithm in Unsteady Process

In order to check the performance of pressure estimation algorithm, the measurement data at various time instances are analyzed. The distribution of pressure and viscosity at corresponding time instances are shown in Fig. 4. The measurement data are at corresponding vortices development stage to separation and migration in downstream. At t=0.06 s, in wake, the shear layer vortices are developing and exactly symmetrical with respect to center of cylinder. Symmetric viscosity and low-pressure regions are obtained downstream in the wake Fig.4(a). At t=12 s, the vortices are developed but still attached with shear layers. The corresponding viscosity and low-pressure region formed accordingly in wake, Fig. 4(b). At t=22 s, vortices are separated from shear layer. The viscosity and pressure distributions are also formed as expected, Fig. 4(c).

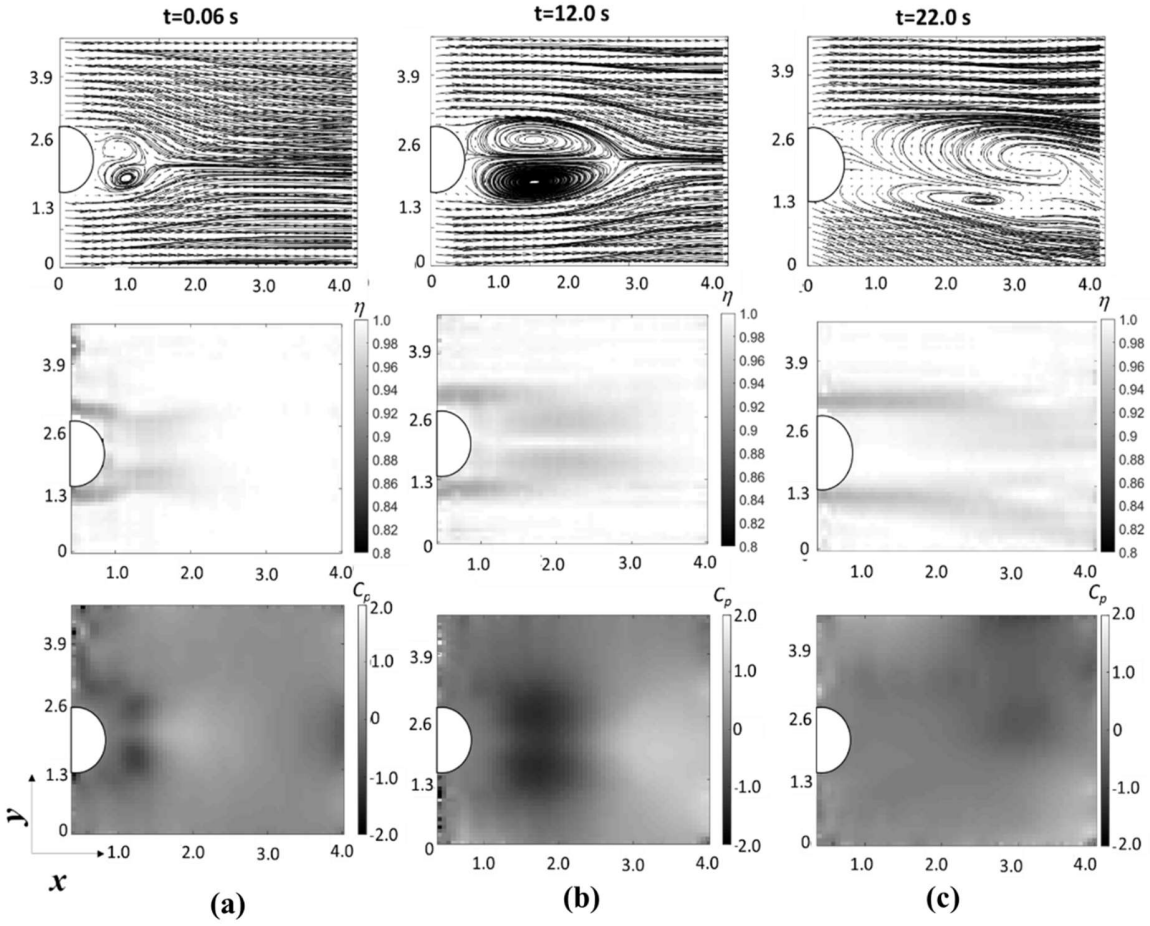

Fig.4 Velocity, viscosity and pressure (Cp) distribution for various time instances (a) t=0.06 s, (b) t=12.0 s and (c) t=22.0 s at U=30mm/s

4.3 Relation Between Material Property to Pressure and Vorticity

Even though vortex flow over cylinder is a widely researched topic, the relation between viscosity and pressure in von-Kármán vortex street is never mentioned in literature. Due to fact that in incompressible flows viscosity under pressure do not change significantly. Here an attempt is made to obtain some relation between viscosity, pressure and enstrophy ($|\omega|^2$) by analyzing their variation in entire computational domain. For several instances the line integral convolution plots are shown in Fig.5(a), these plots clearly show the various stages of vortices development and separation. Along with that, the viscosity variation with pressure and enstrophy in scatter plots are shown in Fig.5(b), (c).

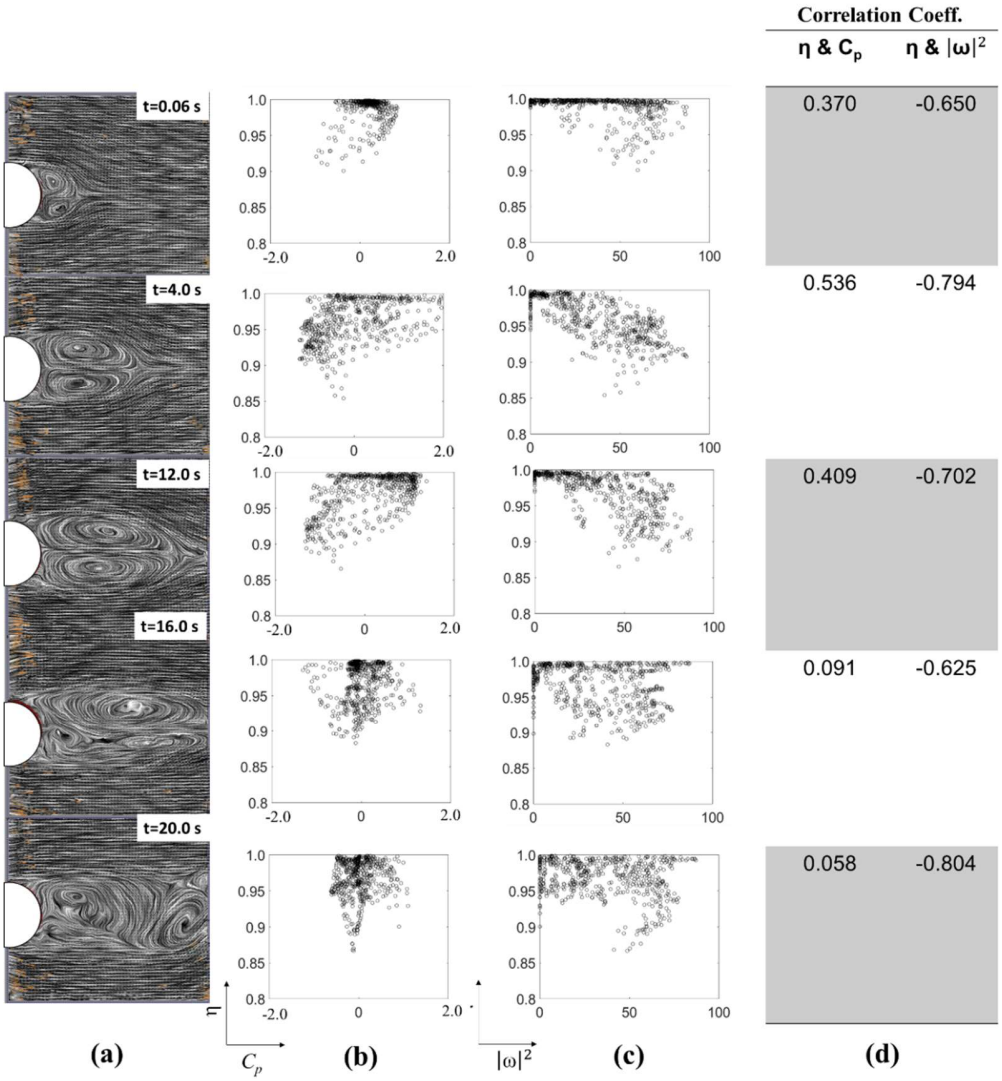

Fig. 5 (a) Line integral convolution plots at time t=0.06 s to 20 s, with correlation plots between (b) viscosity (η) and pressure (Cp) and (c) viscosity (η) vs enstrophy (d) corresponding correlation coefficients given at right.

The corresponding correlation coefficients (Cc) are represented in Fig.5(d).

$$Cc = \frac{1}{N-1}\sum_{i=1}^{N}\left(\frac{\overline{A_i - \zeta_a}}{\sigma_a}\right)\left(\frac{B_i - \zeta_b}{\sigma_b}\right) \tag{11}$$

Here Cc represents the linear dependence of two variable A and B, having N observations. and are mean and standard deviations. In present results the viscosity is negatively correlated with enstrophy and positively correlated with pressure. Quantitatively viscosity is more correlated with enstrophy than the pressure. At several stages of vortex development, separation and after separation, Cc of η Vs $|\omega|^2$ is increases successively. Enstrophy represent the energy dissipation in flow (Zhu and Gao, 2017), it is obvious that as time increases the turbulent kinetic energy dissipation increases and negative correlation indicated decrement in η. Positive correlation of η with Cp shows that as time increases the pressure is also decreases which signifies that the pressure lowering at vortex core is intensified with time due to shear thinning property of fluid.

5 Concluding Remarks

A new approach is presented to evaluate the instantaneous pressure in shear thinning fluid. The measured velocity data, filtered by POD was used in rheological models to evaluate both viscosity and pressure from momentum equation, simultaneously. The power law model and Carreau-Yasuda models are compared. Qualitatively both the models predicted the viscosity distribution in shear layer and wake region accurately. The instantaneous distribution of pressure is successfully obtained with a robustness to the non-Newtonian characteristics. We found that the pressure-lowering in the vortex cores of von Kármán flow was intensified by the shear-thinning property of the fluid, proved by the positive correlation between the local viscosity and the pressure. Moreover, correlation between viscosity and pressure became significantly weaker when vortices starts migrating in wake.

Acknowledgment

This work was financially supported by Japan Society for Promotion of Science (JSPS KAKENHI, 17H01245 and 18KK0105). The authors are thankful to Prof. Eric Windhab, ETHZ, for technical advices.

References

Cross M M (1968) Rheology of viscoelastic fluids: elasticity determination from tangential stress measurement J. Colloid Interface Sci. 27 84–90

Carreau P J (1972) Rheological Equations from Molecular Network Theories Cit. Trans. Soc. Rheol. 16 99

Clermont J-R and Normandin M (1993) Numerical simulation of extrudate swell for Oldroyd-B fluids using the stream-tube analysis and a streamline approximation J. Nonnewton. Fluid Mech. 50 193–215

Walters K and Webster M F (2003) The distinctive CFD challenges of computational rheology Int. J. Numer. Methods Fluids 43 577–96

Tamano S, Itoh M, Kato K and Yokota K (2010) Turbulent drag reduction in nonionic surfactant solutions Phys. Fluids 22 055102

Tasaka Y, Yoshida T, Rapberger R and Murai Y (2018) Linear viscoelastic analysis using frequency-domain algorithm on oscillating circular shear flows for bubble suspensions Rheol. Acta 57 229–40

Shiratori T, Tasaka Y, Oishi Y and Murai Y (2015) Ultrasonic velocity profiling rheometry based on a widened circular Couette flow Meas. Sci. Technol. 26 085302

Yoshida T, Tasaka Y and Murai Y (2017) Rheological evaluation of complex fluids using ultrasonic spinning rheometry in an open container J. Rheol. 61 537–49

Yip R, James D F and Currie I G (2011) PIV measurements of slow flow of a viscoelastic fluid within a porous medium Exp. Fluids 51 801–9

Dey A A, Modarres-Sadeghi Y and Rothstein J P (2018) Viscoelastic fluid-structure interactions between a flexible cylinder and wormlike micelle solution Phys. Rev. Fluids 3 063301

Wiklund J and Stading M (2008) Application of in-line ultrasound Doppler-based UVP–PD rheometry method to concentrated model and industrial suspensions Flow Meas. Instrum. 19 171–9

van Oudheusden B W (2013) PIV-based pressure measurement Meas. Sci. Technol. 24 032001

van der Kindere J W, Laskari A, Ganapathisubramani B and de Kat R (2019) Pressure from 2D snapshot PIV Exp. Fluids 60 32

Murai Y, Nakada T, Suzuki T and Yamamoto F (2007) Particle tracking velocimetry applied to estimate the pressure field around a Savonius turbine Meas. Sci. Technol. 18 2491–503

Srinivasan S and Rajagopal K R (2010) A note on the flow of a fluid with pressure-dependent viscosity in the annulus of two infinitely long coaxial cylinders Appl. Math. Model. 34 3255–63

Thielicke W and Stamhuis E J (2014) PIVlab – Towards User-friendly, Affordable and Accurate Digital Particle Image Velocimetry in MATLAB J. Open Res. Softw. 2

Scarano F and Riethmuller M L (1999) Iterative multigrid approach in PIV image processing with discrete window offset Exp. Fluids 26 513–23

McClure J and Yarusevych S (2017) Optimization of planar PIV-based pressure estimates in laminar and turbulent wakes Exp. Fluids 58 62

Zhu H and Gao Y (2017) Vortex-induced vibration suppression of a main circular cylinder with two rotating control rods in its near wake: Effect of the rotation direction J. Fluids Struct. 74 469–91